



CHORUS

This is the accepted manuscript made available via CHORUS. The article has been published as:

Isostable reduction with applications to time-dependent partial differential equations

Dan Wilson and Jeff Moehlis

Phys. Rev. E **94**, 012211 — Published 11 July 2016

DOI: [10.1103/PhysRevE.94.012211](https://doi.org/10.1103/PhysRevE.94.012211)

Isostable Reduction with Applications to Partial Differential Equations

Dan Wilson and Jeff Moehlis

Department of Mechanical Engineering, University of California, Santa Barbara, CA 93106

Isostables and isostable reduction, analogous to isochrons and phase reduction for oscillatory systems, are useful in the study of nonlinear equations which asymptotically approach a stationary solution. In this work, we present a general method for isostable reduction of partial differential equations, with the potential power to reduce the dimensionality of a nonlinear system from infinity to one. We illustrate the utility of this reduction by applying it to two different models with biological relevance. In the first example, isostable reduction of the Fokker-Planck equation provides the necessary framework to design a simple control strategy to desynchronize a population of pathologically synchronized oscillatory neurons, as might be relevant to Parkinson's disease. Another example analyzes a nonlinear reaction-diffusion equation with relevance to action potential propagation in a cardiac system.

PACS numbers: 02.30.Jr, 87.19.lj, 87.19.Hh, 87.19.lr

I. INTRODUCTION

For more than half a century, phase reduction techniques have been a remarkably powerful tool to aid in the understanding of oscillatory nonlinear dynamical systems, with a wide array of examples spanning the biological, physical, and chemical sciences [1], [2], [3], [4], [5], [6], [7], [8]. Phase reduction provides a convenient means of changing variables in the neighborhood of a stable limit cycle, distilling the essence of a nonlinear system into a phase in relation to the location on the limit cycle, and a phase response curve which describes the effect of an external input on the phase. In recent years, phase reduction has been used to understand phase locking among groups of oscillators, [3], [8], [9], and has been applied in control schemes to break pathological synchronization [7], and to control oscillatory timing [10].

While phase reduction has been exceedingly useful, it can only be applied to dynamical systems with periodic orbits, excluding a large number of nonlinear systems with dynamics that approach an equilibrium solution. For such systems, the notion of isostables, which are sets of initial conditions that share the same asymptotic convergence towards a fixed point [11] (similar to the notion of stable foliations of an attracting manifold, which can also be used when the system dynamics do not approach a fixed point [12], [13]), provides an analogous set of coordinates from which the intrinsic dynamics of the system can be more conveniently understood.

For example, [14] (c.f. [15]) develops the necessary framework for an isostable reduction (analogous to a phase reduction) for finite dimensional ordinary differential equations (ODEs) with dynamics that approach a fixed point. Here, we extend this framework to systems described by time dependent partial differential equations (PDEs) with dynamics that approach stationary solutions by deriving a methodology to calculate isostable response curves, which allows for the understanding of the effect of a perturbation on a system's approach to the stationary solution. Using this reduction strategy allows us to understand a complicated nonlinear PDE in terms of its isostables, reducing the dimensionality of the system from infinity to one and making complicated problems in nonlinear science more computationally and analytically tractable.

Because the isostable reduction proposed in this paper is valid near a single trajectory that approaches a stationary solution, it is perhaps most similar to PDE reduction methods that involve the use of inertial manifolds [16], [17], [18], [19], which represent exponentially attracting, finite dimensional manifolds that can be used to understand an infinite dimensional PDE. However, inertial manifolds can be difficult to identify, and further analysis must be performed in order to understand the response to an external perturbation. Also, isostable reduction does not explicitly require the dynamics to collapse to a lower dimensional manifold, as multiple trajectories can display similar reduced dynamics.

This isostable reduction methodology looks to be a promising tool for the understanding and control of both linear and fully nonlinear PDEs, particularly when the rate and timing of the system's approach to a stationary solution are of interest. We showcase its utility in two different systems with biological applications. The first is in the reduction of a Fokker-Planck equation with the goal of desynchronizing a large population of pathologically synchronized neurons, as might be relevant in the treatment of Parkinson's

disease. The second is in the reduction of a reaction-diffusion equation with relevance to action potential propagation in cardiac systems.

II. ISOSTABLE REDUCTION AND NUMERICAL CALCULATION OF INFINITESIMAL ISOSTABLE RESPONSE CURVES IN INFINITE DIMENSIONS

In this section we detail a method for calculating infinitesimal isostable response curves (iIRCs) in time dependent partial differential equations which asymptotically approach a stationary solution. To begin, consider a weakly perturbed system on the domain Ω

$$\frac{\partial}{\partial t} \mathbf{X}(\mathbf{r}, t) = \mathbf{F}(\mathbf{X}(\mathbf{r}, t), \mathbf{r}) + \mathbf{G}(\mathbf{X}(\mathbf{r}, t)) + \mathbf{p}(\mathbf{r}, t). \quad (1)$$

Here, $\mathbf{X}(\mathbf{r}, t) \in \mathbb{R}^m$ represents the local state in the medium at point \mathbf{r} and time t , $\mathbf{F}(\mathbf{X}(\mathbf{r}, t), \mathbf{r})$ describes the local dynamics at point \mathbf{r} , $\mathbf{G}(\mathbf{X}(\mathbf{r}, t))$ represents spatial coupling throughout the medium (we allow \mathbf{G} to also be a function of derivatives of \mathbf{X} , e.g. advection or diffusion), and $\mathbf{p}(\mathbf{r}, t)$ represents a weak spatiotemporal perturbation. For given boundary conditions, we assume that both J and J^\dagger exist, where $J \equiv \nabla[\mathbf{F}(\mathbf{X}(\mathbf{r}, t), \mathbf{r}) + \mathbf{G}(\mathbf{X}(\mathbf{r}, t))]$ with $\nabla \equiv \partial/\partial \mathbf{X}$ and † denotes the adjoint associated with $\langle \cdot, \cdot \rangle$, the L^2 inner product. For a given initial condition, in the absence of perturbation (i.e. $\mathbf{p}(\mathbf{r}, t) = 0$), suppose that the system follows a known trajectory γ towards a stationary solution $\mathbf{X}_o(\mathbf{r})$ which satisfies $\mathbf{F}(\mathbf{X}_o(\mathbf{r}), \mathbf{r}) + \mathbf{G}(\mathbf{X}_o(\mathbf{r})) = 0$.

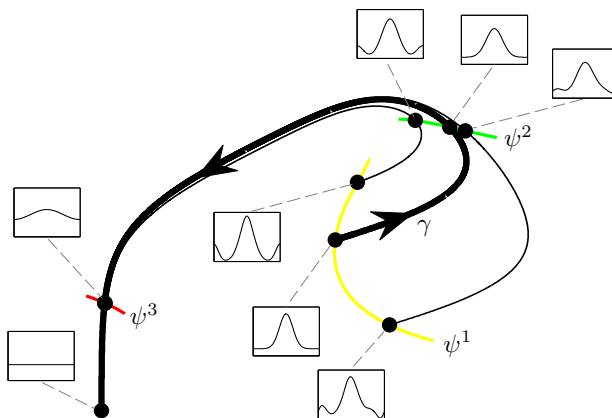


FIG. 1. A qualitative illustration of isostables for a PDE which approaches a stationary solution. Surfaces of constant isostable are represented by colored lines ψ^1 , ψ^2 , and ψ^3 . Black dots represent snapshots of the PDE solution in time. Initial conditions along the same isostable surface approach the fixed point with the same asymptotic convergence as defined by (3). Initial conditions along the same isostable cross successive isostables at the same time. Here, γ is some trajectory for which we wish to characterize the change in isostables in response to spatiotemporal perturbations.

Intuitively, isostables of (1) represent sets of states with the same asymptotic convergence towards the stationary solution [11]. These can be precisely defined using the linearized solution of (1) near the stationary solution. Let ϕ_j be the eigenfunctions of the linearized system, ordered so that ϕ_1 is associated with the eigenvalue λ_1 whose real part has smallest magnitude. In the analysis to follow, we will assume that all eigenvalues have negative real part and that the largest (least negative) eigenvalue is bounded away from both the imaginary axis and the continuous part of the spectrum if it exists. In the simplest case λ_1 is real and unique. If we set $\mathbf{p}(\mathbf{r}, t) = 0$, near the stationary solution functions of constant isostable, I_τ , are given by

$$I_\tau = \left\{ \mathbf{X}(\mathbf{r}) \mid \mathbf{X}(\mathbf{r}) = \mathbf{X}_o(\mathbf{r}) + \pm e^{\lambda_1 \tau} \phi_1 + \sum_{j=2}^{\infty} \alpha_j \phi_j, \quad \forall \alpha_j \in \mathbb{R} \right\}. \quad (2)$$

Here, the amplitude multiplying ϕ_1 determines the isostable, as the amplitudes multiplying the other eigenfunctions decay much faster. Per (2), any linear combination of eigenfunctions ϕ_j for $j \geq 2$ can be added to the current state of the system and will not affect the isostable coordinate of the system.

Equation (2) can only be applied in a close neighborhood of the stationary solution. A fully nonlinear isostable field $\psi = \Psi\{\mathbf{X}(\mathbf{r})\}$ can be defined by considering the infinite time approach of $\mathbf{X}(\mathbf{r}, t)$ with $\mathbf{X}(\mathbf{r}, 0) = \mathbf{X}(\mathbf{r})$ to the stationary solution and computing, for example, [11], [14]

$$\psi = \Psi\{\mathbf{X}(\mathbf{r})\} = \frac{1}{\lambda_1} \log \left(\lim_{t \rightarrow \infty} \left[e^{-\lambda_1 t} \int_{\Omega} \mathbf{Q}^T(\mathbf{r}) (\mathbf{X}(\mathbf{r}, t) - \mathbf{X}_{\mathbf{o}}) d\Omega \right] \right). \quad (3)$$

Here, the isostable functional $\Psi\{\mathbf{X}(\mathbf{r})\}$ maps the state $\mathbf{X}(\mathbf{r}) \in U$ to a scalar isostable (here U is the basin of attraction of $\mathbf{X}_{\mathbf{o}}$), $\mathbf{Q}(\mathbf{r}) \in \mathbb{R}^m$ is a system observable which can be chosen as necessary so that the resulting isostable field gives meaningful information about the system, and T indicates the transpose. See Section II B for an example of how the choice of $\mathbf{Q}(\mathbf{r})$ can influence the isostable field. One can verify that $d\psi/dt = 1$ (c.f. equation 2.3 of [14]) so that in the limit as $\mathbf{X}(\mathbf{r}, t)$ approaches $\mathbf{X}_{\mathbf{o}}$, $\Psi\{\mathbf{X}(\mathbf{r}, t)\}$ approaches ∞ . Figure 1 presents an intuitive sketch of isostables in a nonlinear PDE. Three initial conditions which start at the same isostable coordinate will reach successive isostables at the same time and will have the same asymptotic approach to the stationary solution.

While (3) is useful to precisely define the notion of an isostable, direct calculation of an isostable field using (3) is of limited practical utility. Each state of interest requires direct simulation of (1) to estimate its infinite time approach to the stationary solution which is prohibitively computationally intensive. In practice, however, it can be useful to define an isostable field in a more constructive manner with respect to a single trajectory, γ , by integrating an initial condition forward in time with $\mathbf{p}(\mathbf{r}, t) = 0$ and choosing $\psi(\mathbf{X}(\mathbf{r}, t)) = t$.

As we will show, when $\mathbf{p}(\mathbf{r}, t) \neq 0$, in the limit of weak forcing isostable coordinates provide a convenient means of understanding a system described by a nonlinear PDE in terms of a single ODE through means of an isostable reduction. Following the adjoint method for calculating infinitesimal phase response curves (iPRCs) as used in [20],[14], [8], our goal is to simplify (1) to a one-dimensional equation using scalar isostable coordinates.

To begin, near a known trajectory γ , we take the gradient of the isostable field so that changing to isostable coordinates using the chain rule we find

$$\begin{aligned} \frac{d\psi(\mathbf{X})}{dt} &= \langle \nabla \psi(\mathbf{X}), \partial \mathbf{X} / \partial t \rangle \\ &= \langle \nabla \psi(\mathbf{X}), \mathbf{F}(\mathbf{X}(\mathbf{r}, t), \mathbf{r}) + \mathbf{G}(\mathbf{X}(\mathbf{r}, t)) + \mathbf{p}(\mathbf{r}, t) \rangle \\ &= 1 + \langle \nabla \psi(\mathbf{X}), \mathbf{p}(\mathbf{r}, t) \rangle. \end{aligned} \quad (4)$$

We simplify (4) in the second line using the fact that $d\psi/dt = 1$ when $\mathbf{p}(\mathbf{r}, t) = 0$, thereby implying

$$\langle \nabla \psi(\mathbf{X}), \mathbf{F}(\mathbf{X}(\mathbf{r}, t), \mathbf{r}) + \mathbf{G}(\mathbf{X}(\mathbf{r}, t)) \rangle = 1 \quad (5)$$

for all \mathbf{X} . Evaluating the vector field at $\mathbf{X}^\gamma(\psi)$, which we define as the intersection of the trajectory γ and the $\psi(\mathbf{X})$ level set (i.e. isostable), we have

$$\frac{d\psi(\mathbf{X})}{dt} = 1 + \langle \nabla \psi(\mathbf{X}^\gamma(\psi)), \mathbf{p}(\mathbf{r}, t) \rangle. \quad (6)$$

To proceed, we assume that $\mathbf{p}(\mathbf{r}, t) \equiv 0$ for $t > 0$. Consider a small perturbation $\Delta \mathbf{X}$ at time $t = 0$ to the trajectory $\mathbf{X}(\mathbf{r}, t) \in \gamma$. Letting $\mathbf{X}_\epsilon(\mathbf{r}, t) = \mathbf{X}^\gamma(\mathbf{r}, t) + \Delta \mathbf{X}(\mathbf{r}, t)$ be the perturbed initial condition, we have

$$\frac{\partial \Delta \mathbf{X}(\mathbf{r}, t)}{\partial t} = J(\mathbf{X}(\mathbf{r}, t)) \cdot \Delta \mathbf{X}(\mathbf{r}, t) + \mathcal{O}(\|\Delta \mathbf{X}(\mathbf{r}, t)\|^2), \quad (7)$$

where J is the Jacobian and $(\mathbf{Y} \cdot \mathbf{X})(\mathbf{r}, t) \equiv \mathbf{Y}^T(\mathbf{r}, t) \mathbf{X}(\mathbf{r}, t)$ for any \mathbf{X} and \mathbf{Y} in Ω . We define the isostable shift associated with the perturbation $\Delta \mathbf{X}(\mathbf{r}, t)$ as $\Delta \psi = \psi(\mathbf{X}_\epsilon(\mathbf{r}, t)) - \psi(\mathbf{X}(\mathbf{r}, t))$ and can also write

$$\Delta \psi = \langle \nabla_{\mathbf{X}(\mathbf{r}, t)} \psi, \Delta \mathbf{X}(\mathbf{r}, t) \rangle + \mathcal{O}(\|\Delta \mathbf{X}(\mathbf{r}, t)\|^2), \quad (8)$$

where $\nabla_{\mathbf{X}(\mathbf{r},t)}\psi$ is the gradient of ψ evaluated at $\mathbf{X}(\mathbf{r},t)$. Both Equations (7) and (8) are accurate to leading order in $\Delta\mathbf{X}(\mathbf{r},t)$. After the initial perturbation at $t = 0$, $\Delta\psi$ is independent of time. Taking the time derivative of (8) yields

$$\begin{aligned} \left\langle \frac{\partial \nabla_{\mathbf{X}(\mathbf{r},t)}\psi}{\partial t}, \Delta\mathbf{X}(\mathbf{r},t) \right\rangle &= - \left\langle \nabla_{\mathbf{X}(\mathbf{r},t)}\psi, \frac{\partial \Delta\mathbf{X}(\mathbf{r},t)}{\partial t} \right\rangle \\ &= - \langle \nabla_{\mathbf{X}(\mathbf{r},t)}\psi, J(\mathbf{X}(\mathbf{r},t)) \cdot \Delta\mathbf{X}(\mathbf{r},t) \rangle \\ &= - \langle J(\mathbf{X}(\mathbf{r},t))^\dagger \nabla_{\mathbf{X}(\mathbf{r},t)}\psi, \Delta\mathbf{X}(\mathbf{r},t) \rangle. \end{aligned} \quad (9)$$

Here, $J(\mathbf{X}(\mathbf{r},t))^\dagger$ is the adjoint of the real-valued operator $J(\mathbf{X}(\mathbf{r},t))$. Equation (9) holds for arbitrary perturbations $\Delta\mathbf{X}(\mathbf{r},t)$, which gives the relation

$$\frac{\partial \nabla_{\mathbf{X}(\mathbf{r},t)}\psi}{\partial t} = -J(\mathbf{X}(\mathbf{r},t))^\dagger \nabla_{\mathbf{X}(\mathbf{r},t)}\psi. \quad (10)$$

In practice when J^\dagger is difficult to derive analytically, and it can be estimated numerically by first discretizing (1) and solving for the adjoint of the resulting system of ODEs with appropriate boundary conditions [21]. In this case, the Hermitian transpose of the Jacobian of the discretized ODE system provides an estimate of the adjoint. In order to use (10) one must have knowledge of $\nabla_{\mathbf{X}(\mathbf{r},t)}\psi$ (i.e. the iIRC) at some initial time, which is usually possible by studying the system near the stationary solution, as we illustrate in Section II A.

While isostables and the associated iIRC describe the infinite time approach towards the stationary solution, in practice, most engineering applications can only consider finite time. Therefore, for the one dimensional reduction (4) to be of practical use, $|\lambda_1| - |\lambda_2|$ multiplied by the time scale of interest must be large enough so that higher order modes become negligible. If the time scales are too short for a one dimensional reduction to be effective, one can also use (10) to calculate response curves which characterize the infinite time decay of higher order modes in response to the perturbation $\mathbf{p}(\mathbf{r},t)$. This strategy gives a multi-dimensional reduction with details given in Section II B.

A. Isostable Fields Near a Stationary Solution

In order to solve (10) in the calculation of iIRCs we must know $\nabla_{\mathbf{X}(\mathbf{r},t)}\psi$ at some initial time. This can be accomplished by linearizing around the stable stationary solution, \mathbf{X}_o where in many cases we can determine the isostable field exactly for the linearized equation. We emphasize that the linearization is only required to determine an initial condition for the solution to (10). Upon solving (10), the isostable response curve is valid for the reduction of the full nonlinear equations.

Consider a linearization of (1) near a stationary solution \mathbf{X}_o :

$$\frac{\partial}{\partial t}\mathbf{X} = J(\mathbf{X}_o)(\mathbf{X} - \mathbf{X}_o) + \mathcal{O}((\mathbf{X} - \mathbf{X}_o)^2). \quad (11)$$

Neglecting higher order terms, we can write its solution as an infinite sum of eigenfunctions:

$$\mathbf{X} - \mathbf{X}_o = \sum_{j=1}^{\infty} s_j(\mathbf{X}(0))\phi_j e^{\lambda_j t}. \quad (12)$$

Here, ϕ_j corresponds to an eigenfunction of J with the associated eigenvalue λ_j , and $s_j(\mathbf{X})$ gives the coordinates of function \mathbf{X} in the basis of eigenfunctions $\{\phi_j, j = 1, \dots, \infty\}$. Furthermore, we sort the associated eigenvalues $\{\lambda_j, j = 1, \dots, \infty\}$ so that $|\text{Re}(\lambda_j)| \leq |\text{Re}(\lambda_{j+1})|$.

In the simplest case, λ_1 is real and unique, then the magnitude of $s_1(\mathbf{X})$ will determine the infinite time approach to the stationary solution (c.f. [11]). Using this perspective, a set of isostables, i.e. $\Psi_\tau \equiv \{\mathbf{X} | \Psi\{\mathbf{X}\} = \tau\}$, can be uniquely determined by finding the magnitude of $s_1(\mathbf{X})$. In other words, sets of constant isostables are spanned by the faster eigenfunctions $\phi_2, \phi_3, \phi_4, \dots$, and any perturbations to $s_j(\mathbf{X}(0))$ for $j \geq 2$ will not have any effect on the infinite time approach to the origin. Therefore,

$$\langle \nabla_{\mathbf{X}(\mathbf{r},t)}\psi, \phi_j \rangle = 0 \quad \forall j \geq 2. \quad (13)$$

In the case that λ_1 and $\lambda_2 = \overline{\lambda_1}$ are a complex conjugate pair (with corresponding eigenfunctions ϕ_1 and $\phi_2 = \overline{\phi_1}$, equation (10) is still valid, but the strategy for finding the initial condition changes slightly. Consider an infinite time approach to the linearized stationary solution, given in (12). Assuming that $\text{Re}(\lambda_1) > \text{Re}(\lambda_3)$, as time becomes large, the solution is dominated by the complex eigenfunction pair

$$\mathbf{X} - \mathbf{X}_o = s_1 \phi_1 e^{\lambda_1 t} + \overline{s_1} \overline{\phi_1} e^{\overline{\lambda_1} t} + \mathcal{O}(e^{\lambda_3 t}). \quad (14)$$

Using Euler's formula and algebraic manipulation, equation (14) can be rewritten as

$$\mathbf{X} - \mathbf{X}_o = A e^{\text{Re}(\lambda_1)t} [\cos(\theta_o + \text{Im}(\lambda_1)t) \text{Re}(\phi_1) - \sin(\theta_o + \text{Im}(\lambda_1)t) \text{Im}(\phi_1)] + \mathcal{O}(e^{\lambda_3 t}), \quad (15)$$

where A and θ_o are constants which can be determined from s_1 and $\overline{s_1}$. Therefore, near the stationary solution, functions of constant isostable can be defined as follows (c.f. [11]):

$$I_\tau = \left\{ \mathbf{X}(\mathbf{r}) \in \mathbb{R}^m \mid \mathbf{X}(\mathbf{r}) = e^{\text{Re}(\lambda_1)\tau} [\cos(\theta) \text{Re}(\phi_1) - \sin(\theta) \text{Im}(\phi_1)] + \sum_{j=3}^{\infty} \alpha_j \phi_j, \quad \forall \alpha_j \in \mathbb{R}, \quad \forall \theta \in [0, 2\pi) \right\}. \quad (16)$$

Thus, similar to (13),

$$\begin{aligned} \langle \nabla_{\mathbf{X}(\mathbf{r},t)} \psi, \phi_j \rangle &= 0, \quad \forall j \geq 3 \quad \text{and} \\ \langle \nabla_{\mathbf{X}(\mathbf{r},t)} \psi, w(t) \rangle &= 0 \end{aligned} \quad (17)$$

where $w(t) = \frac{\partial}{\partial t} [\cos(\theta_o + \text{Im}(\lambda_1)t) \text{Re}(\phi_1) - \sin(\theta_o + \text{Im}(\lambda_1)t) \text{Im}(\phi_1)]$. The second orthogonality condition in (17) comes from the fact that the isostable response curve must be orthogonal to I_τ near the stationary solution. A perturbation in the direction $w(t)$ will simply speed up or slow down oscillations about the stationary solution, but will not affect their magnitude (and hence will not affect the isostable).

When λ_1 is real and unique (resp. part of a complex conjugate pair) equation (13) (resp. (17)) defines a unique shape of the isostable response curve near the stationary solution, and the magnitude can be obtained from (5). Thus, in order to determine an initial condition for (10), we can choose a point \mathbf{X}_1 along γ , close enough to the stationary solution so that the $\mathcal{O}((\mathbf{X} - \mathbf{X}_o)^2)$ terms in equation (11) are negligible. With this initial condition, (10) can be solved by integrating backwards in time to determine $\nabla \psi$ for the full nonlinear equations at all points close to γ . The resulting iIRC may vary depending on the specific trajectory γ which must be chosen appropriately for a given application. If the underlying system has fast-slow dynamics that quickly converges to, for instance, an inertial manifold [16], [17], this manifold could be taken to be γ . However, fast convergence to a known trajectory is not required.

B. Higher Dimensional Reductions

Assume that we have a general PDE (1) with a solution that asymptotically approaches a stationary solution, \mathbf{X}_o . We also assume that near \mathbf{X}_o , we may write the solution as an infinite sum of eigenfunctions, ϕ_j and associated eigenvalues λ_j in the same form as (12). Isostables provide a useful means for characterizing a solution's infinite time approach to \mathbf{X}_o (i.e. the infinite time decay of the eigenfunction ϕ_1 associated with the eigenvalue of smallest magnitude), but it could be of practical interest to track the infinite time decay decay along additional eigenfunctions. Here, we illustrate a reduction to N dimensions for the simplest case where $|\lambda_1| < |\lambda_2| < \dots < |\lambda_N|$ and $\lambda_1, \dots, \lambda_N$ are real and negative, but situations with repeated or complex eigenvalues could be considered.

For the PDE (1) on the domain Ω with given boundary conditions, isostables describe the asymptotic convergence of a solution, $\mathbf{X}(\mathbf{r}, t)$ to \mathbf{X}_o . We can define an isostable field in terms of a functional Ψ_1 that maps the state $\mathbf{X}(\mathbf{r}, 0)$ to a scalar isostable (c.f. [14], [11])

$$\Psi_1\{\mathbf{X}(\mathbf{r}, 0)\} \equiv \lim_{t \rightarrow \infty} e^{-\lambda_1 t} \int_{\Omega} |\mathbf{X}(\mathbf{r}, t) - \mathbf{X}_o| d\Omega. \quad (18)$$

Here $\int_{\Omega} \cdot d\Omega$ denotes integration over the entire domain Ω . In infinite time, projections of the solution $\mathbf{X}(\mathbf{r}, t) - \mathbf{X}_o$ onto the eigenfunctions ϕ_2, ϕ_3, \dots become infinitesimally small compared to the projection of

$\mathbf{X}(\mathbf{r}, t) - \mathbf{X}_o$ onto ϕ_1 , so that we can give an equivalent definition of (18)

$$\Psi_1\{\mathbf{X}(\mathbf{r}, 0)\} = \lim_{t \rightarrow \infty} e^{-\lambda_1 t} \int_{\Omega} |w_1(\mathbf{X}(\mathbf{r}, t) - \mathbf{X}_o)| d\Omega, \quad (19)$$

where w_1 gives the projection of $\mathbf{X}(\mathbf{r}, t) - \mathbf{X}_o$ onto ϕ_1 . We can characterize the asymptotic behavior of the projection onto any other eigenfunction ϕ_j , by defining additional functionals

$$\Psi_j\{\mathbf{X}(\mathbf{r}, 0)\} = \lim_{t \rightarrow \infty} e^{-\lambda_j t} \int_{\Omega} |w_j(\mathbf{X}(\mathbf{r}, t) - \mathbf{X}_o)| d\Omega, \quad (20)$$

where w_j gives the projection of $\mathbf{X}(\mathbf{r}, t) - \mathbf{X}_o$ onto ϕ_j . Because $w_j(\mathbf{X}(\mathbf{r}, t) - \mathbf{X}_o) \propto \phi_j e^{\lambda_j t}$ as $t \rightarrow \infty$, one can verify (c.f. equation (2.3) from [14]) that functionals (19) and (20) are defined so that $\psi_j \equiv \log(\Psi_j)/\lambda_j$ defines fields for which

$$\langle \nabla \psi_j(\mathbf{X}), \mathbf{F}(\mathbf{X}(\mathbf{r}), \mathbf{r}) + \mathbf{G}(\mathbf{X}) \rangle = 1. \quad (21)$$

The analysis from Section II can be applied to any of these fields so that for a given trajectory γ , an infinitesimal response curve $\nabla_{\mathbf{X}(\mathbf{r}, t)} \psi_j$, the gradient of ψ_j evaluated at $\mathbf{X}(\mathbf{r}, t)$, can be calculated using (10). Near the stationary solution, any perturbation in the direction ϕ_k for $k \neq j$ will not affect the infinite time behavior of the projection of $\mathbf{X}(\mathbf{r}, t) - \mathbf{X}_o$ onto the eigenfunction ϕ_j . Therefore, near the stationary solution $\nabla_{\mathbf{X}(\mathbf{r}, t)} \psi_j$ satisfies

$$\langle \nabla_{\mathbf{X}(\mathbf{r}, t)} \psi_j, \phi_k \rangle = 0 \quad \text{for } k = 1, 2, \dots, j-1, j+1, j+2, \dots \quad (22)$$

Equations (21) and (22) determine an initial condition for each response curve, and (10) can be used to calculate N response curves for the N eigenfunctions of interest. Even though eigenfunctions do not carry any meaning for the fully nonlinear equations, these response curves still describe how a perturbation will affect the infinite time approach to the stationary solution when the perturbation is applied in the nonlinear regime. This yields the N -dimensional reduction:

$$\frac{d\psi_j}{dt} = 1 + \langle \nabla \psi_j(\mathbf{X}^\gamma(\psi_j)), \mathbf{p}(\mathbf{r}, t) \rangle, \quad j = 1, \dots, N. \quad (23)$$

For $N = 1$, (23) is equivalent to the one-dimensional isostable reduction considered in Section II. When $N > 1$, the reduction characterizes the decay of the projection of the solution $\mathbf{X}(\mathbf{r}, t) - \mathbf{X}_o$ onto the eigenfunctions ϕ_1, \dots, ϕ_N and ignores the higher order modes. Thus, for an N -dimensional reduction we require $|\lambda_1| - |\lambda_N|$ multiplied by the time scale of interest to be large enough so that the truncated modes become negligible. This is in direct contrast to inertial manifold reductions, which require the gap between consecutive eigenvalues to be large [17], [22].

III. APPLICATION TO PARKINSON'S DISEASE AND NEURAL NETWORKS

We consider a model of pathological neural synchronization, thought to contribute to the motor symptoms associated with Parkinson's disease [23], [24], [25]. For patients whose symptoms are drug resistant, Deep Brain Stimulation (DBS) offers an alternative treatment to mitigate these motor symptoms through the injection of a high-frequency, pulsatile input into an appropriate brain region. It has been hypothesized that the functional mechanism of DBS is the desynchronization of these pathologically synchronized brain regions [26], [27]. In recent years, researchers have developed alternative desynchronization strategies [28], [29], [30] that could make DBS more efficient in order to prolong battery life of the implantable device as well as to mitigate potential side effects of DBS [31]. In previous work [7], we developed a methodology for chaotically desynchronizing a population of synchronized oscillators which only required knowledge of the neurons' phase response curves (PRCs). However, this strategy only guarantees desynchronization when the neurons are close in phase, and as a consequence cannot guarantee that a population of will be driven to a splay, or completely desynchronized, state.

Using isostable reduction techniques derived in Section II, we can design an external stimulus to desynchronize a population of neurons by driving them towards the splay state. To begin, we assume that each

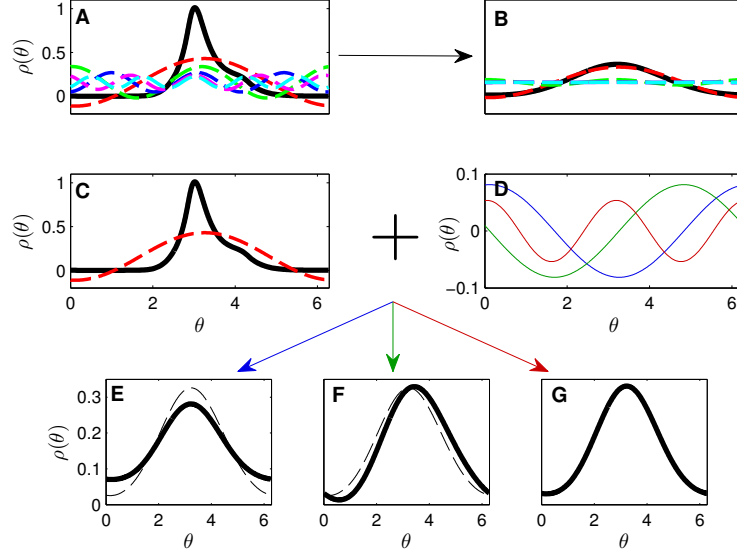


FIG. 2. Illustration of isostables in the advection-diffusion equation. Panel A shows an initial distribution in black and several associated Fourier modes as dashed lines. After some time passes, panel B shows that all other modes except for the first have decayed substantially. Panel C shows the same initial distribution with the first mode shown in red for reference, to which we add one of three perturbations given in panel D. After $4T$ has elapsed, the distribution resulting from the blue, green, and red perturbation is shown as a solid line in panels E, F, and G, respectively, with the unperturbed distribution after $4T$ has elapsed shown as a dashed line. The perturbed and unperturbed distributions are indistinguishable in panel G.

individual neuron from the larger population can be represented as a noisy limit cycle oscillator:

$$\dot{\theta}_j = \omega + Z(\theta_j) \left(u(t) + \frac{1}{N} \sum_{i=1}^N \sigma(V(\theta_i) - V(\theta_j)) + \sqrt{2S} \eta_j(t) \right), \quad j = 1, \dots, N. \quad (24)$$

Equation (24) is an example of a phase reduction, a strategy that has been immensely useful in the understanding of many physical, chemical, and biological systems [1], [5], [4]. Here, $\theta_j \in [0, 2\pi)$ is the 2π -periodic phase of the j^{th} neuron with $\theta = 0$ corresponding to the neuron firing an action potential, $\omega = 2\pi/T$ represents the neuron's baseline frequency and is determined from its natural period T , $Z(\theta)$ is the phase response curve, which gives the change in phase due to an infinitesimal impulsive current, σ is the coupling strength in an all-to-all network, $\sqrt{2S}\eta_j(t)$ is i.i.d. zero mean white noise with intensity $2S$, $u(t) = I(t)/C$ with $I(t)$ being a common external current control input and $C = 1\mu\text{F}/\text{cm}^2$ the constant neural membrane capacitance, N is the total number of neurons, and $V(\theta)$ gives the transmembrane voltage as a function of the phase. We assume S is small enough that higher order noise terms are negligible (c.f. [32]). Also, we assume that the coupling in this network is electrotonic, but this could be generalized to include, for example, chemical synaptic coupling. Assuming that the population is large and noise perturbations are small, with stochastic averaging [33] we can approximate (24) according to its probability density $\rho(\theta, t)$ with the Fokker-Planck equation in one dimension [34]

$$\begin{aligned} \frac{\partial \rho(\theta, t)}{\partial t} &= -\frac{\partial}{\partial \theta} [(\omega + Z(\theta)(u(t) + \sigma(\bar{V} - V(\theta))))\rho(\theta, t)] + \frac{1}{2} \frac{\partial^2}{\partial \theta^2} [B^2 \rho(\theta, t)] \\ &= -\omega \rho_\theta + \frac{B^2}{2} \rho_{\theta\theta} \underbrace{-[Z(\theta)\rho_\theta + Z'(\theta)\rho]u(t)}_{\text{external input}} \underbrace{-\frac{\partial}{\partial \theta} [Z(\theta)\sigma(\bar{V} - V(\theta))\rho]}_{\text{intrinsic coupling}}, \end{aligned} \quad (25)$$

where $\bar{V} = \int_0^{2\pi} V(\theta)\rho(\theta)d\theta$ and $B^2 = \frac{2S}{2\pi} \int_0^{2\pi} Z^2(\theta)d\theta$ represent averaged transmembrane voltage and noise, respectively. For the moment, we will consider (25) in the absence of external input and intrinsic coupling.

Without these terms, we have a linear advection-diffusion equation on a ring, whose eigenfunctions are related to the Fourier modes of the distribution. Panel A of Figure 2 shows an example distribution in black along with several corresponding Fourier modes, shown as dashed lines. After some time passes, all but the first mode has significantly decayed, as shown in panel B. The behavior of this system can be understood from the perspective of isostables, which as outlined in [11] are sets of initial conditions which share the same asymptotic convergence towards a stationary solution, in this case the uniform distribution $\rho = 1/(2\pi)$. As shown for this advective-diffusive system in Appendix A, the magnitude of the first mode determines the isostable, and thereby the asymptotic approach of the system to the stationary solution, because all other modes die out at a faster rate in the presence of noise.

Solutions to (25) exist in infinite dimensional space, and for this reason it can be difficult to work with for control purposes. To reduce the complexity of this equation, one can instead track the change in isostables in response to an external perturbation, with examples given in panels C-G of Figure 2. Panel C shows the probability distribution along with the first mode, for reference, to which we add one of the three perturbations shown in panel D. Panels E, F, and G show the resulting distribution after $4T$ elapses. We find that adding the blue perturbation, which is antiphase to the first mode, results in a faster approach to the stationary solution, as shown in panel E. Adding a perturbation orthogonal to the first mode (shown in green) does not affect the isostable, but shifts the distribution to the right slightly, shown in panel F. Adding a perturbation corresponding to a higher order mode (shown in red) does not effect the system's approach to the stationary solution, shown in panel G.

Using the intuition gleaned from Figure 2, one can understand the essence of the following isostable reduction: in isostable coordinates, (25) becomes

$$\begin{aligned} \dot{\psi} &= 1 + \left\langle \mathcal{I}(\theta, \psi), -[Z(\theta)\rho_\theta + Z'(\theta)\rho]u(t) - \frac{\partial}{\partial\theta}[Z(\theta)\sigma(\bar{V} - V(\theta))\rho] \right\rangle, \\ \mathcal{I}(\theta, \psi) &= \frac{-2}{A_1^* B^2 \pi} \cos(\theta - \varphi_1^* - \omega\psi) e^{\frac{B^2\psi}{2}}. \end{aligned} \quad (26)$$

Here, ψ is the isostable of the system with $\psi \equiv 0$ corresponding to an arbitrary time t^* , $\mathcal{I}(\theta, \psi)$ is the infinitesimal isostable response curve (iIRC), which represents the gradient of the isostable field, $\langle \cdot, \cdot \rangle$ is the L^2 inner product, and $A_1^* \cos(\theta - \varphi_1^*)$ is the first Fourier mode of $\rho(\theta, t^*)$. Complete details of the derivation of this reduction are given in Appendix A. The iIRC for this system is shown in panel B of Figure 3. The magnitude of the iIRC grows exponentially with increasing ψ so that it requires smaller perturbations to influence the isostable of the system as it approaches the stationary solution (c.f. [14]).

Equation (26) is a one dimensional ODE, and is much easier to work with than the infinite dimensional PDE from (25), yet still retains essential characteristics of original equation. Equation (26) can be understood as follows: if the inner product is zero, noise will be responsible for driving the system to larger isostables, which are closer to the stationary, desynchronized distribution. However, the term responsible for internal coupling, $-\frac{\partial}{\partial\theta}[Z(\theta)\sigma(\bar{V} - V(\theta))\rho]$, can counteract the effects of noise, maintaining some level of synchrony in the network. Therefore, we can use the term associated with the external control, $-[Z(\theta)\rho_\theta + Z'(\theta)\rho]u(t)$, to reverse the effects of internal coupling, driving the distribution closer to the stationary solution, thereby desynchronizing the network. Viewing the network from this perspective leads to a novel control strategy, which would not be apparent from the full equations (25). Assuming each neuron receives the same input $u(t)$, and assuming that the maximum and minimum input that can be applied is $u_{\max} \geq 0$ and $u_{\min} \leq 0$, respectively, which may be relevant for hardware or tissue limitations, we can apply the control

$$u(t) = \begin{cases} u_{\max} & \text{if } \langle \mathcal{I}(\theta, \varphi_1(\rho)), -[Z(\theta)\rho_\theta + Z'(\theta)\rho] \rangle > 0, \\ u_{\min} & \text{otherwise.} \end{cases} \quad (27)$$

When this strategy is implemented, the external control serves to maximize the right hand side of (26), driving the system towards higher values of ψ , which correspond to less synchronous population distributions.

We apply the control strategy to a population of neurons, each with intrinsic dynamics characterized by a two dimensional reduction of the Hodgkin-Huxley (HH) equations [35] that reproduces the essential characteristics of the neuron's dynamical behavior, [36], c.f. [37]:

$$\begin{aligned} \dot{V}_j &= f_V(V_j, n_j) + I + \frac{\sigma}{N} \sum_{i=1}^N (V_i - V_j) + u(t) + \eta_j(t), \\ \dot{n}_j &= f_n(V_j, n_j). \end{aligned} \quad (28)$$

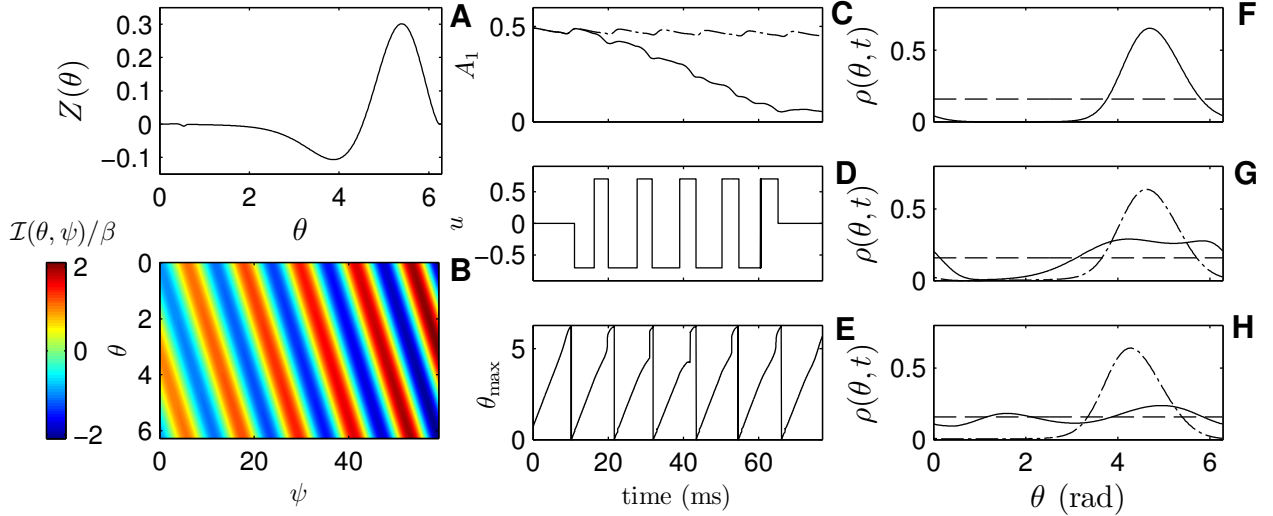


FIG. 3. Isostable reduction applied to the Fokker-Planck equation. Panel A shows $Z(\theta)$, used in the desynchronizing control strategy. Panel B shows the iIRC, $\mathcal{I}(\theta, \psi)/\beta$ where $\beta \equiv 2/A_1^* B^2 \pi$. Panels C-H show the result of applying the control strategy to the PDE (25). The control input (in $\mu\text{A}/\mu\text{F}$) in D drives the first mode of the distribution from 0.5 to 0.05. Panel C gives the amplitude of this mode as a function of time for the equations with control applied as well as the system without control, shown as a solid and dashed-dot line, respectively. Panel E gives the location of the maximum of the distribution, θ_{\max} , as a function of time. Panels F-H show a comparison of the controlled distribution to the uncontrolled distribution at $t = 7.4, 41.8$ and 75.8 ms. The horizontal dashed line shows the ideal, uniform distribution.

Here, f_V and f_n are functions which describe the intrinsic neural dynamics, with all terms and parameters given in [37], $I = 10 \mu\text{A}/\text{cm}^2$ is a baseline current given so that each neuron is in a periodically spiking regime, $j = 1, \dots, N$ where N is the total number of neurons, and V_j and n_j are the transmembrane voltage and gating variable for neuron j , respectively. Note that (24) can be obtained from (28) through phase reduction. The phase response curve, $Z(\theta)$, which gives the change in phase due to an infinitesimal impulsive current stimulus is calculated using the software XPP [38] and is shown in panel A of Figure 3. To test our control strategy (27), we take the coupling strength σ to be 0.06 and a white noise intensity $2S = 2$, (with the resulting value $B^2 = 0.0251$), and $u_{\max} = -u_{\min} = 0.7 \mu\text{A}/\mu\text{F}$. The specific values of u_{\max} and u_{\min} can be changed without reducing the effectiveness of the control strategy provided they are large enough to overcome the synchronizing effects of intercellular coupling, but small enough that the phase reduction (24) is valid [5].

In the absence of external control, the internal coupling will cause a large population of neurons to approach a distribution that is periodic in time, shown at a particular snapshot in panel F of Figure 3. Starting with this distribution, we simulate the reduced PDE (25) with our control strategy. The resulting control is shown in panel D of Figure 3. Panels F-H show snapshots of the controlled distribution as solid lines with the uncontrolled distribution shown as a dot-dashed line for reference. We find that the applied control drives the system close to a uniform distribution with a stimulus that is close to periodic. This is useful because the control strategy (27) requires knowledge of the underlying distribution, which is generally unavailable when simulating the full neural network (28). Instead we can make the following observations about the desynchronizing control to design a simple closed loop control strategy: 1) The average voltage of the system achieves a maximum value approximately when $\theta_{\max} = 2\pi$. 2) Each time $\theta_{\max} = 2\pi$, the external control is at u_{\min} . 3) The control transitions from u_{\min} to u_{\max} at approximately 6.1 ms after $\theta_{\max} = 2\pi$. 4) The control remains at u_{\max} for approximately 3.7 ms before transitioning back to u_{\min} . Figure 4 gives a direct comparison of the dynamics of the full PDE system (25) and the isostable reduced dynamics (26) under the application of the desynchronizing control (27). The isostable field is appropriately shifted so that the state $\rho(\theta, 0)$ corresponds to $\psi = 0$. The desynchronizing control strategy is applied between 15 and 70 ms. Recall that the magnitude of the iIRC grows as the isostable increases (see panel B of Figure 3), so that the growth rate of ψ appears exponential, even though the magnitude of the applied control remains unchanged.

Without control, the coupling maintains an isostable value near zero (not shown).

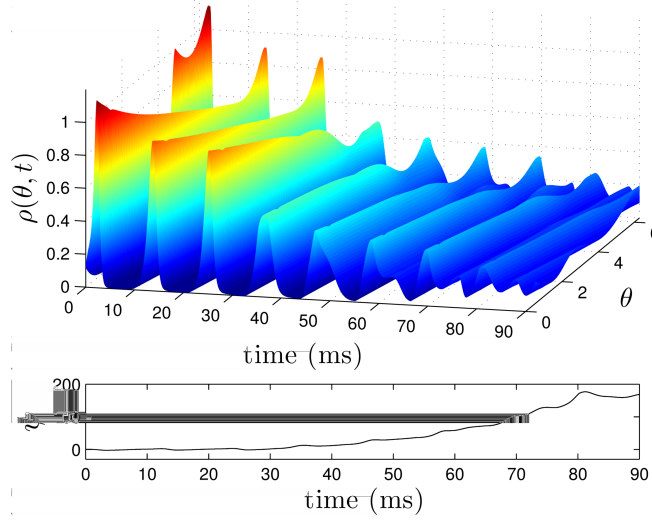


FIG. 4. The top and bottom panels shows the state of the full equations (25) and the reduced equations (26) with control (27). Larger isostable values correspond to more desynchronized states.

These observations allow for the design of the following control strategy for use in the full neural equations. Monitor the average voltage, $\bar{V} = \sum_{j=1}^N V_j$, of the system. Let t_{spike} denote the most recent time \bar{V} reaches a local maximum which is above -50 mV, denoting that $\theta_{\text{max}} \approx 2\pi$, and apply the control

$$u = \begin{cases} u_{\text{max}} & \text{if } 3.7 < t - t_{\text{spike}} < 9.8, \\ 0 & \text{if } t - t_{\text{spike}} > 15, \\ u_{\text{min}} & \text{otherwise.} \end{cases} \quad (29)$$

Notice that if the average voltage remains low enough, the controller is simply turned off. We can apply this control when the average voltage spikes above -50 mV, and turn the controller off until the population has resynchronized.

We apply (29) to a population of $N = 300$ neurons, shown in the top panel of Figure 5 where the black lines give individual neural traces for 30 representative neurons from the population, and the red line gives the average voltage for the system. We find that the applied control (middle panel), quickly desynchronizes the system, as can be seen from the Kuramoto order parameter [5], shown in the bottom panel (for the splay state, $R = 0$). Turning off the controller allows the neurons to resynchronize, at which point the controller can be turned on again to desynchronize the system. We note that the control strategy which produces chaotic desynchronization from [7] cannot desynchronize the population with this parameter set. This happens because individual cells tend to break off from the synchronized population, quickly travel around the limit cycle, and rejoin the synchronized population before it can desynchronize.

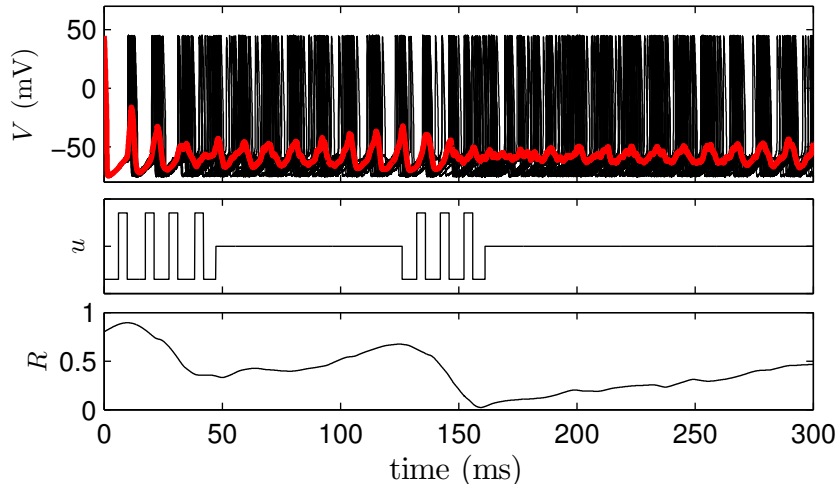


FIG. 5. The top panel shows the approximated control strategy (29) applied to a population of Hodgkin-Huxley neurons, with the middle and bottom panels showing the applied control and the Kuramoto order parameter, R , for the network, respectively.

IV. APPLICATION TO A NONLINEAR PDE

Consider a one dimensional reaction-diffusion system of length L , which might be used to model action potential propagation in an excitable system such as the heart [39], [40]:

$$\frac{\partial}{\partial t} u(r, t) = D \frac{\partial^2}{\partial r^2} u(r, t) + I_{\text{int}}(r, t) + I_{\text{ext}}(r, t). \quad (30)$$

Here u is a voltage-like variable which might represent transmembrane potential, r represents the spatial location, $D = 2$ is the diffusion constant, $I_{\text{ext}}(r, t)$ represents an external perturbation to $V(r, t)$, and $I_{\text{int}}(r)$ is determined by local dynamics. We take no-flux boundary conditions and use a modified FitzHugh-Nagumo model of excitable dynamics (c.f. [41]) so that

$$\begin{aligned} I_{\text{int}}(r, t) &= c_1 u(r, t)(u(r, t) - a)(1 - u(r, t)) - c_2 v(r, t)u(r, t), \\ \frac{\partial}{\partial t} v(r, t) &= b(u(r, t) - dv(r, t)), \end{aligned} \quad (31)$$

Here, v might represent a gating variable of an excitable cell membrane. We take constants $a = 0.1$, $b = 0.005$, $c_1 = 1$, $c_2 = 1$, $d = 2.5$, and $L = 500$. In the absence of external perturbations, the model dynamics eventually settle to the stationary solution at $u(r) = 0$, $v(r) = 0$. When the system is at the stationary solution, a large enough positive external perturbation to the u variable will create a pulse which cascades throughout the system and dies out at the boundaries. Using isostable reduction, we can understand how perturbations will affect the wave speed and can use this information to predict behavior in models with higher spatial dimension. For convenience, we will choose $\psi = 0$ to correspond to the moment the traveling wave is initiated in the medium.

Starting from the stationary solution, we set $u(r, 0) = 1$ for $r \leq 4$ to initiate a traveling wave in the medium. The resulting initial conditions are used to integrate (30) forward in time for 1400 units of time with $I_{\text{ext}} \equiv 0$, and the resulting trajectory is taken to be γ . Figure 6 provides three snapshots of the state at three different isostables. The wave travels from left to right before being absorbed by the boundary, at which point the voltage-like variable v quickly approaches zero and the variable u approaches zero more slowly. Equation (30) is a nonlinear PDE, and unlike in the previous example from Section III, an isostable response curve will be calculated numerically using (10). To write (30) in the form of equation (1) in order to calculate an iIRC, let $\mathbf{X}(r, t) = [u(r, t), v(r, t)]^T$ and $F(\mathbf{X}) = [c_1 u(u - a)(1 - u) - c_2 v u, b(u - dv)]^T$. Also, let $G(\mathbf{X}(r, t))$ be diffusive coupling in the variable u , leaving $\mathbf{p}(r, t) = [I_{\text{ext}}, 0]^T$. The corresponding isostable

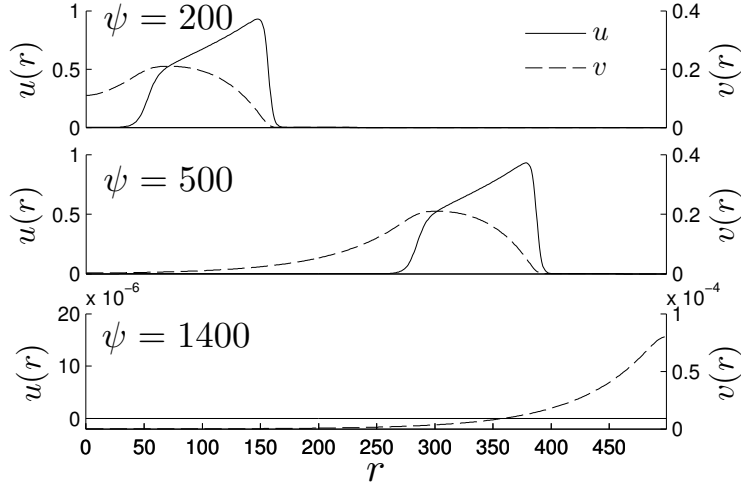


FIG. 6. At $\psi = 0$ a perturbation to u creates a traveling wave in the excitable system. The wave is absorbed by the right boundary. The variable v approaches the stationary solution slowly relative to u .

reduction for this system is

$$\dot{\psi} = 1 + \langle \mathcal{I}_u(r, \psi), I_{\text{ext}}(r, \psi) \rangle + \langle \mathcal{I}_v(r, \psi), 0 \rangle. \quad (32)$$

For completeness, we explicitly acknowledge $\mathcal{I}_v(r, \psi)$ even though we cannot directly perturb the variable v .

At $t = 1400$, the traveling wave has died out and the state of the system is close enough to the stationary solution so that it can be approximated by the linearization about the stationary solution:

$$\frac{\partial}{\partial t} u(r, t) = D \frac{\partial^2}{\partial r^2} u(r, t) + I_{\text{int}}(r, t), \quad (33)$$

$$I_{\text{int}}(r, t) = -c_1 a u(r, t), \quad (34)$$

$$\frac{\partial}{\partial t} v(r, t) = b u(r, t) - b v(r, t). \quad (35)$$

In the linearized equations, $v(r)$ is only present in (35), and one can verify that any function of the form $[u(r) = 0, v(r)]^T$ is an eigenfunction of the linearized system with associated eigenvalue $\lambda_1 = -bd$. Numerically, using a central space discretization [42] of the diffusive term in (33), we find that the eigenvalues of the remaining eigenfunctions are real and larger in magnitude than $|\lambda_1|$. Therefore, there are an infinite number of eigenfunctions corresponding to the slowest direction of the stable manifold which span the function space $v(r)$. This is similar to the situation described in Section II B, and an isostable response curve could be defined for each of these eigenfunctions. However, we will only be interested in a single eigenfunction: $\phi = [u(r), v(r)]^T$ with $u(r) = 0$ and $v(r) = 1$ if $r = L$ and $v(r) = 0$ otherwise. Here ϕ describes the approach of $v(L)$ to zero. The associated iIRC describes the effect of an external perturbation on the wave speed (i.e. a perturbation which speeds up the wave will ultimately cause the system to decay to the steady state solution more quickly). Recall from (22) that for a given eigenfunction associated with a real eigenvalue, near the stationary solution the iIRC is orthogonal to the remaining eigenfunctions, with magnitude normalized so that it satisfies (5). Using this information, the iIRC is approximated near the stationary solution with the eigenvectors of a discretized system [21], and then the iIRC is calculated by solving (10) backwards in time. The resulting iIRC is valid for the fully nonlinear equation (30).

Figure 7 shows the numerically calculated iIRC for this system at $\psi = 200$ (200 time units after the creation of the traveling wave). The top-left and top-right panels show the iIRC for perturbations to the variable u and v , respectively. The dashed line shows $u(r)$ at $\psi = 200$ for reference. At other values of ψ for which the traveling wave is sufficiently far from the boundaries the iIRCs do not change magnitude or shape, but rather, are translated at the wave speed, numerically calculated to be 0.77 units of distance per

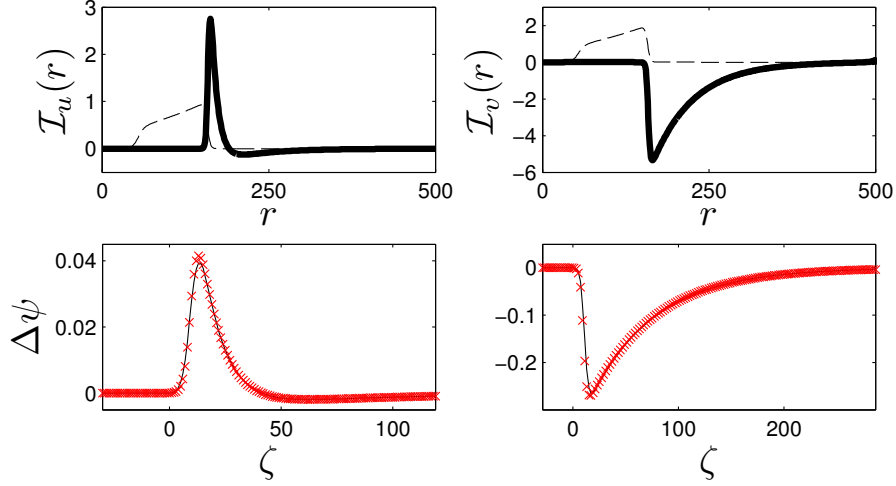


FIG. 7. Top-left and top-right panels show the iIRC at $\psi = 200$ as solid lines for perturbations to u and v , respectively. Dashed lines show $u(r)$ for reference. Bottom left and right panels compare theoretical predictions (black lines) to results from direct numerical simulation (red crosses) for perturbations to $u(r)$ and $v(r)$, respectively. Here, the variable ζ represents the signed distance from where the perturbation is centered relative to the peak of $u(r)$.

unit of time. In order to verify $\mathcal{I}_u(r)$, direct perturbations of the form

$$u(r, t^+) = \begin{cases} u(r, t^-) + A & \text{if } |\zeta - r| \leq 2, \\ u(r, t^-) & \text{otherwise,} \end{cases} \quad (36)$$

are given at time t where $A = 0.003$ denotes the magnitude of the perturbation and ζ denotes the location where $u(r)$ takes its maximum (which from Figure 7 is close to the point at which $\mathcal{I}_u(r)$ is maximized). Resulting changes in isostables are measured through direct numerical simulation by comparing the time at which the pulse reaches the boundary with and without perturbation. Individual datapoints are shown as red crosses and agree well with theoretical predictions based on the iIRC's. Direct perturbations to $v(r)$ of the same form as (36) but with $A = 0.01$ are given and results are shown in the bottom-right panel of Figure 7.

With these results in mind, we consider the behavior of a two dimensional excitable system

$$\frac{\partial}{\partial t} u(\mathbf{s}, t) = \nabla \cdot \bar{\sigma} \nabla u(\mathbf{s}, t) + I_{\text{int}}(r) + I_{\text{ext}}(\mathbf{s}, t), \quad (37)$$

with no-flux boundary conditions and local dynamics that follow (31). Here, $\mathbf{s} = [x, y]$ and the diagonal matrix $\bar{\sigma} = \text{diag}([D_x, D_y])$ is a conductivity tensor allowing for anisotropy in the medium, a common feature when modeling cardiac action potential propagation [43]. Here we will take the domain to be rectangular with L_x and L_y representing the lengths in the x and y directions, respectively. In the following analysis, we will find that the long term behavior of traveling waves in this system can be understood using isostable reduction. Particularly, when one spatial direction is much smaller than the other, the wave front will self-align so that it is perpendicular to the longer direction. To begin, we discretize (37) *in the x spatial direction only* into a system of N coupled PDEs

$$\begin{aligned} \frac{\partial}{\partial t} u^1(y, t) &= D_y \frac{\partial^2}{\partial y^2} u^1(y, t) + I_{\text{int}}^1(y) + \frac{D_x}{\Delta x^2} (u^2(y, t) - u^1(y, t)), \\ \frac{\partial}{\partial t} u^i(y, t) &= D_y \frac{\partial^2}{\partial y^2} u^i(y, t) + I_{\text{int}}^i(y) \\ &\quad + \frac{D_x}{\Delta x^2} [(u^{i+1}(y, t) - u^i(y, t)) + (u^{i-1}(y, t) - u^i(y, t))], \quad i = 2, \dots, N-1, \\ \frac{\partial}{\partial t} u^N(y, t) &= D_y \frac{\partial^2}{\partial y^2} u^N(y, t) + I_{\text{int}}^N(y) + \frac{D_x}{\Delta x^2} (u^{N-1}(y, t) - u^N(y, t)), \end{aligned} \quad (38)$$

with $\Delta x = L_x/(N-1)$. With this particular discretization, notice that each PDE is of the same form as (30) if we define, for instance, $I_{\text{ext}}^i \equiv \frac{D_x}{\Delta x^2} [(u^{i+1}(y, t) - u^i(y, t)) + (u^{i-1}(y, t) - u^i(y, t))]$ for $i = 2, \dots, N-1$. For these identical coupled PDEs, we can define a trajectory γ common to each PDE which will be used to define an isostable reduction. We assume that external perturbations are small enough so that each cell remains close to γ and that to leading order ϵ there is a 1-to-1 relationship between ψ_i and the state variables $u_i(r)$ and $v_i(r)$. The system of PDEs (30) can then be reduced to isostable coordinates as follows

$$\begin{aligned}\dot{\psi}^1 &= 1 + \frac{D_x}{\Delta x^2} \langle I_u(y, \psi^1), u(y, \psi^2) - u(y, \psi^1) \rangle, \\ \dot{\psi}^i &= 1 + \frac{D_x}{\Delta x^2} \langle I_u(y, \psi^i), u(y, \psi^{i+1}) - u(y, \psi^i) + u(y, \psi^{i-1}) - u(y, \psi^i) \rangle, \quad i = 2, \dots, N-1, \\ \dot{\psi}^N &= 1 + \frac{D_x}{\Delta x^2} \langle I_u(y, \psi^N), u(y, \psi^{N-1}) - u(y, \psi^N) \rangle.\end{aligned}\tag{39}$$

Notice that (39) is a function of each isostable in the system. Furthermore, we find through direct numerical evaluation, when the wave is sufficiently far from the boundaries of the one dimensional subsystems, $\langle I_u(y, \psi^1), (u(y, \psi^2) - u(y, \psi^1)) \rangle$ can be reduced to a function of the form $f(\varphi^1)$ where $\varphi^i \equiv \psi^{i+1} - \psi^i$, shown as a black line in panel A of Figure 8, calculated using $L_y = 1000$ units and $D_y = 2$. Using this new definition, we can rewrite (39) in terms of the evolution of the phase differences

$$\begin{aligned}\dot{\varphi}^1 &= \frac{D_x}{\Delta x^2} (2f(\varphi^1) - f(\varphi^2)), \\ \dot{\varphi}^i &= \frac{D_x}{\Delta x^2} (-f(\varphi^{i-1}) + 2f(\varphi^i) - f(\varphi^{i+1})), \quad i = 1, \dots, N-2 \\ \dot{\varphi}^{N-1} &= \frac{D_x}{\Delta x^2} (2f(\varphi^{N-1}) - f(\varphi^{N-2})).\end{aligned}\tag{40}$$

Because $f(0) = 0$, equation (40) has a fixed point at $[\varphi^1, \dots, \varphi^{N-1}] = [0, \dots, 0]$. Linearizing about this fixed point and letting $k = df/d\varphi|_{\varphi=0}$, we arrive at

$$\begin{aligned}\dot{\varphi}^1 &= \frac{kD_x}{\Delta x^2} (2k\varphi^1 - k\varphi^2), \\ \dot{\varphi}^i &= \frac{kD_x}{\Delta x^2} (-k\varphi^{i-1} + 2k\varphi^i - k\varphi^{i+1}), \quad i = 1, \dots, N-2, \\ \dot{\varphi}^{N-1} &= \frac{kD_x}{\Delta x^2} (2k\varphi^{N-1} - k\varphi^{N-2}).\end{aligned}\tag{41}$$

In the limit as Δx approaches 0, $[\varphi^1, \varphi^2, \dots, \varphi^{N-1}]$ can be approximated by the continuous function $\Phi(x, t)$ where, for example, $\int_0^{k\Delta x} \Phi(s, t) ds \approx \varphi^1 + \dots + \varphi^k = \psi^{k+1} - \psi^1$. In this limit, (41) is well approximated by

$$\frac{\partial}{\partial t} \Phi(x, t) = -kD_x \frac{\partial^2}{\partial x^2} \Phi(x, t),\tag{42}$$

with $x \in [0, L_x]$, $\Phi(0, t) = \Phi(L_x, t) = 0$. The solution to (42) is given by [44]

$$\Phi(x, t) = \sum_{n=1}^{\infty} B_n \sin\left(\frac{n\pi x}{L_x}\right) \exp\left(-\frac{kD_x n^2 \pi^2}{L_x^2} t\right),\tag{43}$$

with the coefficients B_n defined according to initial conditions. The results of this analysis indicate when the isostable values are nearly identical so that the phase difference coupling $f(\varphi)$ is small enough, the Fourier modes of $\Phi(x, t)$ decay exponentially at a rate determined by kD_x . Panels B-E of Figure 8 show a simulation of (37) with D_x, D_y, L_x , and $L_y = 0.1, 2.0, 50$, and 1000, respectively. For this choice of parameters, k is numerically determined to be -1.036. A wave is initiated at the top of the domain with an external perturbation to u at $x = L_x/2$. Two snapshots are shown in Panel B at $t = 400$ and $t = 1200$, denoted by a \diamond and $*$, respectively. Panel C gives the difference in isostables as a function of x at these two times. Here $\bar{\psi}$ is the average isostable of the system at a given time. Solid lines in Panels D and E show the maximum isostable difference as a function of time. Panel E highlights the behavior near the end of the simulation. The dashed red line denotes the expected behavior, based on (43) and the red dot denotes the point at which the theoretical comparison begins. As the isostables converge, the theoretical predictions agree well with numerical observations.

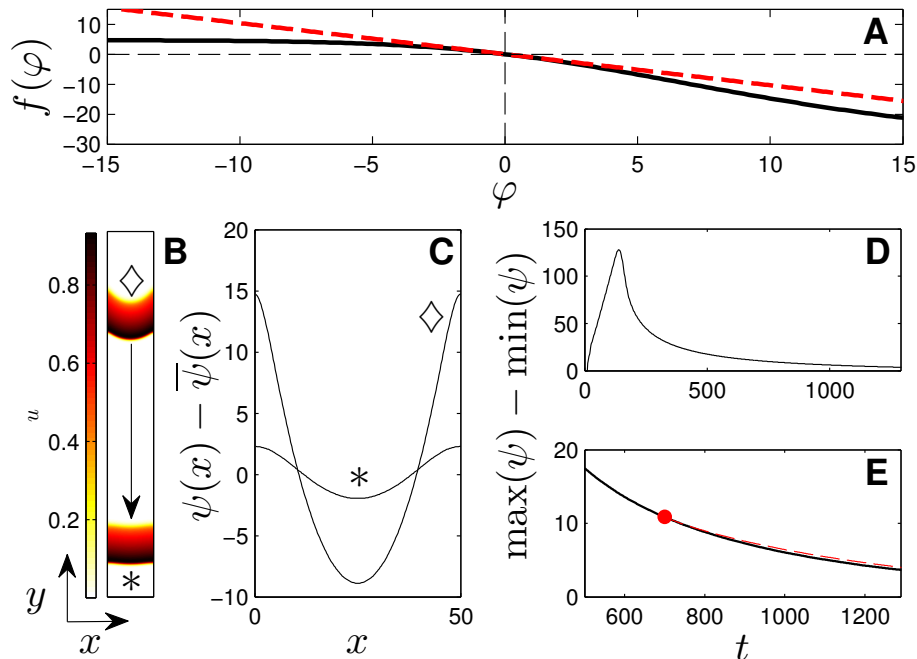


FIG. 8. Panel A shows the numerically calculated isostable difference coupling from (40). The red dashed line gives $f(\varphi)$ linearized about $\varphi = 0$, as used in (41). Panel B shows snapshots of a traveling wave at two points in time in the 2D system (37). The isostable difference as a function of x (the shorter dimension) is plotted in panel C for the snapshots from panel B. Black lines from panels D and E show the numerically calculated maximum difference in isostables as a function of time. The dashed red line in panel E is calculated from (43) using numerically determined isostable data at $t = 700$ as an initial condition.

V. DISCUSSION

State reduction can be a powerful strategy for both understanding and controlling systems with complicated and high dimensional dynamics. Here, we have developed a methodology of state reduction for PDEs which tracks the time it takes for an initial condition to reach a stable stationary solution in the presence of external inputs. To illustrate both the power and flexibility of this method, we have applied it to problems from two different fields of study.

In the first application, isostable reduction allows us to design an input to desynchronize a large population of phase oscillators. This control strategy could have potential applications to Parkinson's disease, where excessive synchrony in a network of neurons is thought to contribute to the motor symptoms of the disease. While this control strategy represents a significant improvement over previous ones, it will certainly need to be developed further before it can be applied *in vivo*. For instance, the control strategy (27) requires simultaneous monitoring and stimulation of the network dynamics, an issue that will need to be addressed in practice. While increased synchronization is not the only pathological change associated with Parkinson's disease, and desynchronization may not alleviate all symptoms, control strategies based on mitigating the excessive synchrony associated with Parkinson's disease have shown promise in both human and primate studies [45], [46].

In a second application, we analyze a nonlinear PDE with relevance to wave propagation in reaction-diffusion systems. In this case, isostable reduction allows us to reduce the long term behavior of a nonlinear system with two spatial dimensions to a simple diffusive process in one spatial dimension. The isostable reduction methodology naturally extends to more complicated models of excitable dynamics and may be useful in the design of electrical therapies for cardiac arrhythmias such as alternans [14], [47], [40] or in the study of waves of spreading depression associated with migraines [48], [49].

Isostable reduction is not the only reduction strategy that can be applied to PDEs. This method of isostable

reduction is perhaps most similar to reduction through the use of inertial manifolds [16], [17], [18], [19] which attract solutions of PDEs exponentially quickly. While inertial manifolds are an important analytical tool for analyzing high dimensional systems, they can be difficult to approximate, and it is not guaranteed that a resulting inertial manifold would be low dimensional. Furthermore, once an inertial manifold is found, further analysis would need to be performed in order to understand how small perturbations affect the dynamics. The isostable reduction strategy described in this work does not explicitly require the state dynamics to collapse to a one-dimensional manifold.

Future work could address strategies for reducing PDEs for which the least negative eigenvalue of the linearized system is part of a continuous spectrum. In this work, we explicitly exclude this possibility so that viewing the dynamics in terms of a finite set of isostable coordinates would be sufficient to characterize the long term behavior of a given PDE. If the least negative eigenvalue belongs to a continuous spectrum, one would most likely need to consider an infinite set of isostable coordinates associated with a continuous subset of the spectrum to ensure that the truncated isostable dynamics accurately characterize the long term dynamics of the full PDE. Another application of interest would be to investigate the convergence of a PDE to a periodic orbit [8], [40], [50]. In this case, the methodology presented in this manuscript would need to be adapted for use when the dynamics approach a stable periodic orbit rather than a stationary solution.

Phase reduction has played an important role in the understanding of nonlinear oscillatory dynamics in the past half century, and we imagine that isostable reduction could play a similarly important role in the understanding of nonlinear PDEs by allowing for the study of complicated systems in a more useful coordinate system. Isostable reduction allowed us to make progress on a problem with applications to neuroscience, and we imagine that it could be a useful reduction strategy in other contexts, especially when the rate and timing of a system's approach towards a stationary solution are of interest.

Support for this work by National Science Foundation Grant NSF-1363243 and NSF-1264535 is gratefully acknowledged.

Appendix A ISOSTABLE REDUCTION OF THE FOKKER-PLANCK EQUATION

Using isostable reduction techniques, we can design an external stimulus to desynchronize a population of neurons by bringing them closer to the splay state. To begin, we assume that the population can be represented as a set of noisy limit cycle oscillators

$$\dot{\theta}_j = \omega + Z(\theta_j) \left(u(t) + \frac{1}{N} \sum_{i=1}^N \sigma(V(\theta_i) - V(\theta_j)) + \sqrt{2S} \eta_j(t) \right), \quad j = 1, \dots, N. \quad (\text{A1})$$

Here, $\theta \in [0, 2\pi)$ is the 2π -periodic phase of the neuron, $\omega = 2\pi/T$ represents the neuron's baseline frequency and is determined from its natural period T , $\sqrt{2S} \eta_j(t)$ is i.i.d zero mean white noise with intensity $2S$, $u(t) = I(t)/C$ with $I(t)$ being a common external current control input and $C = 1\mu\text{F}/\text{cm}^2$ the constant neural membrane capacitance, and $V(\theta)$ gives the transmembrane voltage as a function of the phase. We assume S is small enough that higher order noise terms are negligible [32]. Also, we assume that the coupling in this network is electrotonic, but this could be generalized to include, for example, chemical synaptic coupling in the network. The coupling is all-to-all with a strength determined by σ . For a large population, it is useful to track the probability density of neurons with phase θ at a given time, $\rho(\theta, t)$. In this case, the coupling in (A1) can be written as $\sigma(\bar{V} - V(\theta_j))$, where $\bar{V} = \int_0^{2\pi} V(\theta) \rho(\theta, t) d\theta$, rather than as a finite sum. In the limit that noise perturbations are small, through stochastic averaging, [33], we can approximate (A1) as

$$\dot{\theta}_j = \omega + Z(\theta_j)(u(t) + \sigma(\bar{V} - V(\theta_j))) + B \eta_j(t), \quad (\text{A2})$$

where $B^2 = \frac{2S}{2\pi} \int_0^{2\pi} Z^2(\theta) d\theta$. For a population of neurons described by (A2), and each receiving an identical input $u(t)$, the probability density evolves according to [34]:

$$\begin{aligned} \frac{\partial \rho(\theta, t)}{\partial t} &= -\frac{\partial}{\partial \theta} [(\omega + Z(\theta)(u(t) + \sigma(\bar{V} - V(\theta)))) \rho(\theta, t)] + \frac{1}{2} \frac{\partial^2}{\partial \theta^2} [B^2 \rho(\theta, t)] \\ &= -\omega \rho_\theta + \frac{B^2}{2} \rho_{\theta\theta} \underbrace{-[Z(\theta) \rho_\theta + Z'(\theta) \rho] u(t)}_{\text{external input}} \underbrace{-\frac{\partial}{\partial \theta} [Z(\theta) \sigma(\bar{V} - V(\theta)) \rho]}_{\text{intrinsic coupling}}. \end{aligned} \quad (\text{A3})$$

For the moment, we will analyze (A3) in the absence of external input or intrinsic coupling in order to perform an isostable reduction on the system, where the stable stationary solution is $\rho(\theta) = 1/(2\pi) = \bar{\rho}$. Without these terms, we have a linear advection-diffusion equation on a ring:

$$\rho_t = M\rho, \quad (\text{A4})$$

where $M \equiv -\omega \frac{\partial}{\partial \theta} + \frac{B^2}{2} \frac{\partial^2}{\partial \theta^2}$. The eigenfunctions and eigenvalues of (A4) are

$$\phi_{2n-1,2n} = e^{\pm in\theta}, \quad \lambda_{2n-1,2n} = -\frac{B^2 n^2}{2} \mp \omega ni. \quad (\text{A5})$$

The infinite time approach to the origin will be governed by the eigenfunctions associated with eigenvalues with the smallest magnitude real part,

$$\rho(\theta, t) - \bar{\rho} = \sum_{n=1}^{\infty} \left[s_{2n-1} e^{in\theta} e^{(-\frac{B^2 n^2}{2} - \omega ni)t} + s_{2n} e^{-in\theta} e^{(-\frac{B^2 n^2}{2} + \omega ni)t} \right], \quad (\text{A6})$$

where the constants $\{s_1, s_2, \dots\}$ are determined by the initial distribution $\rho(\theta, 0)$. Equation (A6) can be rewritten using Euler's formula and the knowledge that the solution is strictly real as

$$\begin{aligned} \rho(\theta, t) - \bar{\rho} &= \sum_{n=1}^{\infty} \left[(a_n \sin(n(\theta - \omega t)) + b_n \cos(n(\theta - \omega t))) e^{-\frac{B^2 n^2}{2} t} \right] \\ &= \sum_{n=1}^{\infty} \left[A_n \cos(n(\theta - \omega t) - \varphi_n) e^{-\frac{B^2 n^2}{2} t} \right], \end{aligned} \quad (\text{A7})$$

where a_n and $b_n \in \mathbb{R}$, $\tan(\varphi_n) = a_n/b_n$ and $A_n = \sqrt{a_n^2 + b_n^2}$, and the second line of (A7) is obtained through trigonometric identities. Equation (A7) mandates that the infinite time approach to the stationary solution will be governed by the magnitude of the first mode of the Fourier expansion of the initial distribution $\rho(\theta, 0)$. Here, because λ_1 is complex, the infinite time approach to the stationary solution is governed by two linearly independent eigenfunctions, $\sin(\theta)$ and $\cos(\theta)$ which spiral towards the stationary solution. A perturbation in the direction $-\sin(\theta - \omega t - \varphi_1)$ perturbs in the direction of the spiral and will not change the isostable on which the function lies. Conversely, perturbations in the orthogonal direction, $\cos(\theta - \omega t - \varphi_1)$, represent the gradient of the isostable field. Examples of the effect of these types of perturbations are shown in Panels C-G of Figure 2 from the main text. With this information and using equation (5), by arbitrarily defining $\psi = 0$ to correspond to time t^* , we have the initial condition

$$\mathcal{I}(\theta, 0) = -\frac{2}{A_1^* B^2 \pi} \cos(\theta - \varphi_1^*), \quad (\text{A8})$$

where $\mathcal{I}(\theta, \psi) \equiv \nabla \psi$ is the isostable response curve and $A_1^* \cos(\theta - \varphi_1^*)$ is the first Fourier mode of the distribution $\rho(\theta, t^*)$. The Jacobian is identical to the operator M for the linear system. Therefore, according to (10), the isostable response curve along an unperturbed trajectory, γ , will change in time according to

$$\frac{d\mathcal{I}}{dt} = -M^\dagger \mathcal{I} = -\omega \mathcal{I}_\theta - \frac{B^2}{2} \mathcal{I}_{\theta\theta}, \quad (\text{A9})$$

where $M^\dagger = \omega \frac{\partial}{\partial \theta} + \frac{B^2}{2} \frac{\partial^2}{\partial \theta^2}$ is the adjoint of the operator M . Using (A9) and (A8) we can explicitly solve for the iIRC

$$\mathcal{I}(\theta, \psi) = \frac{-2}{A_1^* B^2 \pi} \cos(\theta - \varphi_1^* - \omega \psi) e^{\frac{B^2 \psi}{2}}. \quad (\text{A10})$$

Equation (A10) is valid provided that an external input is small enough so that it does not drive the distribution far from γ , the expected trajectory towards the stationary solution, which in this example is given by equation (A7). If the input does drive the system far from γ , the isostable response curve at a given time can be found from the distribution $\rho(\theta, t)$ subject to (A8).

Using the isostable response curve, we can write an isostable reduction of (A3) as

$$\dot{\psi} = 1 + \left\langle \mathcal{I}(\theta, \psi), -[Z(\theta)\rho_\theta + Z'(\theta)\rho]u(t) - \frac{\partial}{\partial\theta}[Z(\theta)\sigma(\bar{V} - V(\theta))\rho] \right\rangle. \quad (\text{A11})$$

-
- [1] A. Winfree. *The Geometry of Biological Time*. Springer Verlag, New York, second edition, 2001.
- [2] G. B. Ermentrout and N. Kopell. Multiple pulse interactions and averaging in systems of coupled neural oscillators. *Journal of Mathematical Biology*, 29(3):195–217, 1991.
- [3] I. Z. Kiss, C. G. Rusin, H. Kori, and J. L. Hudson. Engineering complex dynamical structures: sequential patterns and desynchronization. *Science*, 316:1886–1889, 2007.
- [4] F. C. Hoppensteadt and E. M. Izhikevich. *Weakly Connected Neural Networks*. Springer, New York, 1997.
- [5] Y. Kuramoto. *Chemical Oscillations, Waves, and Turbulence*. Springer-Verlag, Berlin, 1984.
- [6] G. B. Ermentrout and D. H. Terman. *Mathematical Foundations of Neuroscience*, volume 35. Springer, New York, 2010.
- [7] D. Wilson and J. Moehlis. Optimal chaotic desynchronization for neural populations. *SIAM Journal on Applied Dynamical Systems*, 13(1):276–305, 2014.
- [8] H. Nakao, T. Yanagita, and Y. Kawamura. Phase-reduction approach to synchronization of spatiotemporal rhythms in reaction-diffusion systems. *Physical Review X*, 4(2):021032, 2014.
- [9] D. Wilson and J. Moehlis. An energy-optimal approach for entrainment of uncertain circadian oscillators. *Biophysical Journal*, 107(7):1744–1755, 2014.
- [10] K. Serkh and D. B. Forger. Optimal schedules of light exposure for rapidly correcting circadian misalignment. *PLoS Computational Biology*, 10(4):e1003523, 2014.
- [11] A. Mauroy, I. Mezić, and J. Moehlis. Isostables, isochrons, and Koopman spectrum for the action–angle representation of stable fixed point dynamics. *Physica D: Nonlinear Phenomena*, 261:19–30, 2013.
- [12] N. Fenichel. Asymptotic stability with rate conditions. *Indiana Univ. Math. J.*, 23(1109–1137):74, 1973.
- [13] S. Wiggins. *Normally Hyperbolic Invariant Manifolds in Dynamical Systems*. Number 105. Springer, New York, 1994.
- [14] D. Wilson and J. Moehlis. Extending phase reduction to excitable media: Theory and applications. *SIAM Review*, 57(2):201–222, 2015.
- [15] A. J. Roberts. Appropriate initial conditions for asymptotic descriptions of the long term evolution of dynamical systems. *The Journal of the Australian Mathematical Society. Series B. Applied Mathematics*, 31(01):48–75, 1989.
- [16] P. Constantin, C. Foias, B. Nicolaenko, and R. Temam. *Integral Manifolds and Inertial Manifolds for Dissipative Partial Differential Equations*, volume 70. Springer, New York, 1989.
- [17] C. Foias, G. R. Sell, and R. Temam. Inertial manifolds for nonlinear evolutionary equations. *Journal of Differential Equations*, 73(2):309–353, 1988.
- [18] C. Foias, M. S. Jolly, I. G. Kevrekidis, G. R. Sell, and E. S. Titi. On the computation of inertial manifolds. *Physics Letters A*, 131(7):433–436, 1988.
- [19] M. S. Jolly, I. G. Kevrekidis, and E. S. Titi. Approximate inertial manifolds for the Kuramoto-Sivashinsky equation: analysis and computations. *Physica D: Nonlinear Phenomena*, 44(1):38–60, 1990.
- [20] E. Brown, J. Moehlis, and P. Holmes. On the phase reduction and response dynamics of neural oscillator populations. *Neural Computation*, 16(4):673–715, 2004.
- [21] J. P. Keener. *Principles of Applied Mathematics*. Addison-Wesley, Redwood City, California, 1988.
- [22] J. Mallet-Paret and G. R. Sell. Inertial manifolds for reaction diffusion equations in higher space dimensions. *Journal of the American Mathematical Society*, 1(4):805–866, 1988.
- [23] C. Chen, V. Litvak, T. Gilbertson, A. Kühn, C. S. Lu, S. T. Lee, C. H. Tsai, S. Tisch, P. Limousin, M. Hariz, and P. Brown. Excessive synchronization of basal ganglia neurons at 20 Hz slows movement in Parkinson’s disease. *Experimental Neurology*, 205(1):214–221, 2007.
- [24] A. Pogosyan, F. Yoshida, C. C. Chen, I. Martinez-Torres, T. Foltynie, P. Limousin, L. Zrinzo, M. I. Hariz, and P. Brown. Parkinsonian impairment correlates with spatially extensive subthalamic oscillatory synchronization. *Neuroscience*, 171(1):245–257, 2010.
- [25] T. Wichmann, M. R. DeLong, J. Guridi, and J. A. Obeso. Milestones in research on the pathophysiology of Parkinson’s disease. *Movement Disorders*, 26(6):1032–1041, 2011.
- [26] C. Hammond, H. Bergman, and P. Brown. Pathological synchronization in Parkinson’s disease: networks, models and treatments. *Trends Neurosci.*, 30:357–64, 2007.
- [27] P. Tass. *Phase Resetting in Medicine and Biology: Stochastic Modelling and Data Analysis*. Springer, New York, 2007.
- [28] P. Tass. Desynchronizing double-pulse phase resetting and application to deep brain stimulation. *Biol. Cybern.*, 85:343–354, 2001.

- [29] A. Nabi, M. Mirzadeh, F. Gibou, and J. Moehlis. Minimum energy desynchronizing control for coupled neurons. *Journal of Computational Neuroscience*, 34:259–271, 2013.
- [30] M. Rosenblum and A. Pikovsky. Controlling synchronization in an ensemble of globally coupled oscillators. *Physical Review Letters*, 92(11):114102, 2004.
- [31] A. L. Benabid, S. Chabardes, J. Mitrofanis, and P. Pollak. Deep brain stimulation of the subthalamic nucleus for the treatment of Parkinson’s disease. *The Lancet Neurology*, 8(1):67–81, 2009.
- [32] C. Ly and G. B. Ermentrout. Synchronization dynamics of two coupled neural oscillators receiving shared and unshared noisy stimuli. *Journal of Computational Neuroscience*, 26(3):425–443, 2009.
- [33] M. I. Freidlin and A. D. Wentzell. *Random Perturbations of Dynamical Systems*, volume 260. Springer, 2012.
- [34] C. W. Gardiner. *Handbook of Stochastic Methods: for Physics, Chemistry and the Natural Sciences*. Springer, Berlin, 2004.
- [35] A. L. Hodgkin and A. F. Huxley. A quantitative description of membrane current and its application to conduction and excitation in nerve. *J. Physiol.*, 117:500–44, 1952.
- [36] J. Rinzel. Excitation dynamics: insights from simplified membrane models. In *Federation Proceedings*, volume 44, pages 2944–2946, 1985.
- [37] J. Moehlis. Canards for a reduction of the Hodgkin-Huxley equations. *J. Math. Biol.*, 52:141–53, 2006.
- [38] G. B. Ermentrout. *Simulating, Analyzing and Animating Dynamical Systems: A Guide to XPPAUT for Researchers and Students*. SIAM, Philadelphia, 2002.
- [39] A. Garzón, R. O. Grigoriev, and F. H. Fenton. Model-based control of cardiac alternans in Purkinje fibers. *Physical Review E*, 84(4):041927, 2011.
- [40] W.J. Rappel, F. Fenton, and A. Karma. Spatiotemporal control of wave instabilities in cardiac tissue. *Physical Review Letters*, 83(2):456, 1999.
- [41] J. Rogers and A. McCulloch. A collocation-Galerkin finite element model of cardiac action potential propagation. *IEEE Transactions on Biomedical Engineering*, 41:743–757, 1994.
- [42] J. C. Strikwerda. *Finite Difference Schemes and Partial Differential Equations*. SIAM, 2004.
- [43] M. S. Spach. Anisotropy of cardiac tissue. *Journal of Cardiovascular Electrophysiology*, 10(6):887–890, 1999.
- [44] R. Haberman. *Partial Differential Equations with Fourier Series and Boundary Value Problems*. Prentice Hall, New Jersey, 2004.
- [45] I. Adamchic, C. Hauptmann, U. B. Barnikol, N. Pawelczyk, O. Popovych, T. T. Barnikol, A. Silchenko, J. Volkman, G. Deuschl, W. G. Meissner, M. Maarouf, V. Sturm, H. J. Freund, and P. A. Tass. Coordinated reset neuromodulation for Parkinson’s disease: proof-of-concept study. *Movement Disorders*, 29(13):1679–1684, 2014.
- [46] P. A. Tass, L. Qin, C. Hauptmann, S. Dovero, E. Bezard, T. Boraud, and W. G. Meissner. Coordinated reset has sustained aftereffects in parkinsonian monkeys. *Annals of Neurology*, 72(5):816–820, 2012.
- [47] D. J. Christini, M. L. Riccio, C. A. Cuianu, J. J. Fox, A. Karma, and R. F. Gilmour Jr. Control of electrical alternans in canine cardiac Purkinje fibers. *Physical Review Letters*, 96(10):104101, 2006.
- [48] M. Lauritzen, J. P. Dreier, M. Fabricius, J. A. Hartings, R. Graf, and A. J. Strong. Clinical relevance of cortical spreading depression in neurological disorders: migraine, malignant stroke, subarachnoid and intracranial hemorrhage, and traumatic brain injury. *Journal of Cerebral Blood Flow & Metabolism*, 31(1):17–35, 2011.
- [49] A. C. Charles and Serapio M S. M. Baca. Cortical spreading depression and migraine. *Nature Reviews Neurology*, 9(11):637–644, 2013.
- [50] M. Hildebrand, J. Cui, E. Mihaliuk, J. Wang, and K. Showalter. Synchronization of spatiotemporal patterns in locally coupled excitable media. *Physical Review E*, 68(2):026205, 2003.